The Unperturbed Oxo−Sulfido Functional Group *cis*-$Mo^{VI}OS$ Related to That in the Xanthine Oxidase Family of Molybdoenzymes: Synthesis, Structural Characterization, and Reactivity Aspects

Anders Thapper,[†,‡] James P. Donahue,[†] Kristin B. Musgrave,[§] Michael W. Willer,[†] Ebbe Nordlander,[‡] Britt Hedman,*[,§] Keith O. Hodgson,*[,§] and R. H. Holm*[,†]

Department of Chemistry and Chemical Biology, Harvard University, Cambridge, Massachusetts 02138, Department of Chemistry and Stanford Synchrotron Radiation Laboratory, SLAC, Stanford University, Stanford, California, and Inorganic Chemistry I, Chemical Center, Lund University, S-22100 Lund, Sweden

Received April 23, 1999

The oxo-sulfido functional group *cis*-$Mo^{VI}OS$ is essential to the activity of the xanthine oxidase family of enzymes but has proven elusive to synthesis in molecules containing no other four-electron ligands. A direct route to molecules containing this group has been achieved. The reaction system $[MoO_2(OSiPh_3)_2]$/L in dichloromethane yields the complexes $[Mo^{VI}O_2(OSiPh_3)_2L]$ (L = phen (**1**), Me_4phen (**2**), 4,4′-Me_2bpy (**3**), 5,5′-Me_2bpy (**4**), 2 py (**5**)) (74−96%), which are shown to have a distorted octahedral structure of crystallographically imposed C_2 symmetry (**1**, **5**) with cis oxo and trans silyloxy ligands. The related reaction system $[MoO_3S]^{2-}$/$2Ph_3SiCl$/L in acetonitrile affords the complexes $[Mo^{VI}OS(OSiPh_3)_2L]$ (L = phen (**6**), Me_4phen (**7**), 4,4′-Me_2bpy (**8**), 5,5′-Me_2bpy (**9**)) (36−69%). From the collective results of elemental analysis, mass spectrometry, ^{1}H NMR, and X-ray structure determinations (**6**, **7**), complexes **6**−**9** are shown to contain the *cis*-$Mo^{VI}OS$ group in molecules with the same overall stereochemistry as dioxo complexes **1**−**5**. The crystal structures of **6** and **7** exhibit O/S disorder, which was modeled in refinements with 50% site occupancies. The Mo═O (1.607(5) (**6**), 1.645(5) (**7**) Å) and Mo═S (2.257(3) (**6**), 2.203(2) (**7**) Å) bond distances obtained in this way are somewhat shorter and longer, respectively, than expected. Distances obtained by molybdenum EXAFS analysis using the GNXAS protocol for **6**−**9** (Mo═O 1.71−1.72 Å; Mo═S 2.18−2.19 Å) are considered more satisfactory and are in good agreement with EXAFS values for xanthine oxidase. Molybdenum K-edge data for **1** and **6**−**9** are reported. Reaction of **7** with Ph_3P in dichloromethane results in sulfur abstraction and formation of $[Mo^{V}OCl(OSiPh_3)_2(Me_4phen)]$ (**10**), which has a distorted octahedral structure with cis O/Cl and cis silyloxy ligands. Sulfur rather than oxygen abstraction is favored by relative Mo═O/Mo═S bond strengths. Complexes **6**−**9** should allow exploration of the biologically significant *cis*-$Mo^{VI}OS$ group.

Introduction

In their fully oxidized forms, members of the xanthine oxidase family of enzymes contain the oxo−sulfido functional group *cis*-$Mo^{VI}OS$ chelated by one pterin dithiolene cofactor ligand (S_2pd),[1−3] a matter directly verified by EXAFS[4−6] and X-ray crystallography.[7] The group is essential for catalytic activity; the desulfo form is inactive.[8,9] Enzyme activity can be reconstituted, however, in the presence of sulfide under reducing conditions.[10] In a recent mechanistic proposal for xanthine oxidase,[1,7,11] the sulfido ligand in the oxidized site $[Mo^{VI}OS(S_2pd)(OH)]$ acts as a hydride acceptor in the course of nucleophilic attack of hydroxide on the substrate, resulting in the formation of the $Mo^{IV}(O)SH$ unit and product. The reduced site is then oxidized by two electrons to regenerate the oxidized catalytic site. The aldehyde oxidoreductase from *Desulfovibrio gigas* (*Dg*) is the only member of the xanthine oxidase family characterized by crystallography. The structures of the cofactor ligand and the oxidized and reduced forms of the active *Dg* enzyme are shown schematically in Figure 1. The distorted square pyramidal stereochemistry with the sulfido/hydrosulfido ligand in the axial position was established by crystallography.[7] Bond distances are from EXAFS analyses of xanthine oxidase.[1,4−6] An inactive form of *Dg* aldehyde oxidoreductase contains the $Mo^{VI}O_2$ group in which oxo takes the place of the sulfido ligand.[12]

While the structural and reactivity features of the related biologically relevant units $Mo^{VI}O_2$, $Mo^{IV,V}O$, and $Mo^{IV,V}S$ are relatively well developed,[13,14] the *cis*-$Mo^{VI}OS$ group, as dis-

[†] Harvard University.
[‡] Lund University.
[§] Stanford University.

(1) Hille, R. *Chem. Rev.* **1996**, *96*, 2757.
(2) Romão, M. J.; Huber, R. *Struct. Bonding* **1998**, *90*, 69.
(3) For a useful comparison of molybdenum enzyme structures, see: Kisker, C.; Schindelin, H.; Baas, D.; Rétey, J.; Meckenstock, R. U.; Kroneck, P. M. H. *FEMS Microbiol. Rev.* **1999**, *22*, 503.
(4) Cramer, S. P.; Wahl, R.; Rajagopalan, K. V. *J. Am. Chem. Soc.* **1981**, *103*, 7721.
(5) Cramer, S. P.; Hille, R. *J. Am. Chem. Soc.* **1985**, *107*, 8164.
(6) Hille, R.; George, G. N.; Eidsness, M. K.; Cramer, S. P. *Inorg. Chem.* **1989**, *28*, 4018.
(7) Huber, R.; Hof, P.; Duarte, R. O.; Moura, J. J. G.; Moura, I.; Liu, M.-Y.; LeGall, J.; Hille, R.; Archer, M.; Romão, M. J. *Proc. Natl. Acad. Sci. U.S.A.* **1996**, *93*, 8846.
(8) Massey, V.; Edmondson, D. *J. Biol. Chem.* **1970**, *245*, 6595.
(9) Gutteridge, S.; Tanner, S. J.; Bray, R. C. *Biochem. J.* **1978**, *175*, 887.
(10) Wahl, R. C.; Rajagopalan, K. V. *J. Biol. Chem.* **1982**, *257*, 1354.
(11) Hille, R.; Rétey, J.; Bartlewski-Hof, U.; Reichenbecher, W.; Schink, B. *FEMS Microbiol. Rev.* **1999**, *22*, 489.
(12) Romão, M. J.; Archer, M.; Moura, I.; Moura, J. J. G.; LeGall, J.; Engh, R.; Schneider, M.; Hof, P.; Huber, R. *Science* **1995**, *270*, 1170.

10.1021/ic990440v CCC: $18.00
Published on Web 08/20/1999

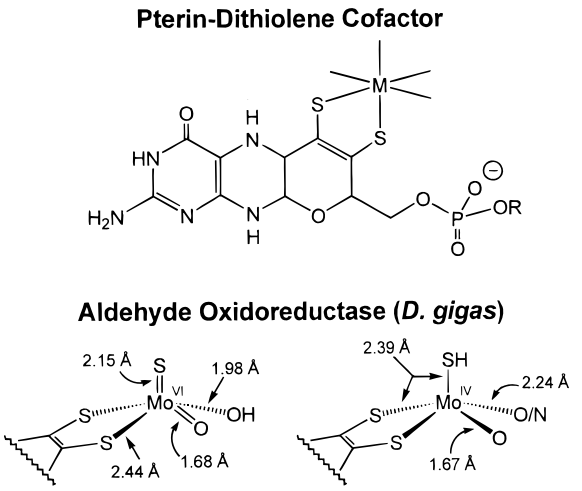

Figure 1. Structures of the pterin dithiolene cofactor (M = Mo, W; R is absent or is a nucleotide) and the reduced and oxidized active sites of *D. gigas* aldehyde oxidoreductase, a member of the xanthine oxidase family. The square pyramidal stereochemistry with the sulfur atom in an axial position was established by protein crystallography.[7] Bond distances are from EXAFS of xanthine oxidase.[1,4−6]

cussed previously,[13] has proved to be an elusive synthetic target in five- or six-coordinate molecules where, as in the enzymes, the remaining binding sites are occupied by *two-electron* ligands.[15−20] This group may be present in six-coordinate [Mo^{V}-$OS(N_2S_2)$], for which, however, there is no XAS evidence for a conventional Mo═S bond (ca. 2.15 Å).[21] In a material formulated as a physical mixture of $[MoO_2Cl_2(OPPh_3)_2]$ and $[MoOSCl_2(OPPh_3)_2]$, the group is indicated as present in one component with Mo−O = 1.67(1) Å and Mo−S = 2.249(7) Å.[22] It is present in $[(HB(Me_2pz)_3)MoOS(\eta^1\text{-}S_2PR_2)]$ (R = Pr^i, Ph)[23,24] and in the organometallic complex $[(C_5Me_5)MoOS(CH_2\text{-}SiMe_3)]$, which is disordered in the crystalline state.[25] In $[(HB(Me_2pz)_3)MoOS(\eta^1\text{-}S_2PPr^i_2)]$, terminal sulfido ligation is perturbed (and presumably stabilized) by the intramolecular cyclic interaction Mo═S···S═P(S)R_2 with Mo═S and S···S distances of 2.227(2) and 2.396(3) Å, respectively.[23] The fundamental chemical and structural properties of the *cis*-Mo^{VI}-OS group could be examined in more detail than presently feasible if it were available, preferably in an unperturbed condition, in five- or six-coordinate complexes. As part of our ongoing investigation of the synthesis and properties of molecules related to the active sites of molybdo-[26,27] and tungstoenzymes,[26,28] we have sought methods for the preparation of the *cis*-$Mo^{VI}OS$ group incorporated in such complexes. Our results, including synthesis, structural characterization by X-ray diffraction and molybdenum EXAFS analysis, and certain reactivity features, are reported here. In this initial investigation, we have not required that the products of synthesis possess the mono(dithiolene) ligation of the active sites of the xanthine oxidase family (Figure 1).

Experimental Section

Preparation of Compounds. All reactions and manipulations were performed under a pure dinitrogen atmosphere using modified Schlenk techniques or an inert-atmosphere box. Commercial samples of 4,4′-dimethyl-2,2′-bipyridine and 5,5′-dimethyl-2,2′-bipyridine were sublimed (160 °C/0.1 Torr). Other reagents were of commercial origin and were used as received. Acetonitrile, dichloromethane, pyridine, and triethylamine were distilled from CaH_2 and stored over 4 Å molecular sieves. In IR spectra, ν_{SiO} features were assigned on the basis of position and intensity; ν_{MoO} bands could not always be located or unambiguously assigned.

$[MoO_2(OSiPh_3)_2(phen)]$. A solution of 0.097 g (0.538 mmol) of 1,10-phenanthroline (phen) in 1 mL of dichloromethane was added to a solution of 0.280 g (0.413 mmol) of $[MoO_2(OSiPh_3)_2]$[29] in 3 mL of dichloromethane. A white precipitate appeared within seconds. Ether (10 mL) was added to the mixture to complete the precipitation. The solid was collected by filtration, washed with 10 mL of acetonitrile and 10 mL of ether, and dried in vacuo. The product was obtained as 0.342 g (96%) of a white solid. IR (KBr): ν_{SiO} 939 cm^{-1} (br), ν_{MoO} 908, 897 cm^{-1}. Absorption data (CH_2Cl_2): λ_{max} (ϵ_M) 272 (24 200), 294 (sh, 10 600), 328 (sh, 1100) nm. ^1H NMR ($CDCl_3$): δ 9.28 (dd, 2,9-H), 8.09 (dd, 4,7-H), 7.59 (s, 5,6-H), 7.41 (dd, 3,8-H). Anal. Calcd for $C_{48}H_{38}MoN_2O_4Si_2$: C, 67.12; H, 4.46; Mo, 11.17; N, 3.26. Found: C, 66.95; H, 4.41; Mo, 11.28; N, 3.18.

$[MoO_2(OSiPh_3)_2(Me_4phen)]$. A solution of 0.088 g (0.372 mmol) of 3,4,7,8-tetramethyl-1,10-phenanthroline (Me_4phen**)** in 1 mL of dichloromethane was added to a solution of 0.233 g (0.343 mmol) of $[MoO_2(OSiPh_3)_2]$ in 2 mL of dichloromethane. Addition of 15 mL of ether gave a white precipitate, which was collected and washed as in the above procedure. The product was obtained as 0.285 g (91%) of a white solid. IR (KBr): ν_{SiO} 941 cm^{-1} (br), ν_{MoO} 910, 897 cm^{-1}. ^1H NMR ($CDCl_3$): δ 9.04 (s, 2,9-H), 7.78 (s, 5,6-H), 2.54, 2.28 (2 s, 3,4,7,8-Me). Anal. Calcd for $C_{52}H_{46}MoN_2O_4Si_2$: C, 68.25; H, 5.07; Mo, 10.48; N, 3.06. Found: C, 68.34; H, 5.06; Mo, 10.63; N, 3.03.

$[MoOS(OSiPh_3)_2(phen)]$. A solution of 0.540 g (1.83 mmol) of Ph_3-SiCl in 10 mL of acetonitrile was added dropwise to a stirred suspension of 0.260 g (1.02 mmol) of $K_2[MoO_3S]$[30] and 0.290 g (1.61 mmol) of phen in 5 mL of acetonitrile containing 1 mL of triethylamine. The reaction mixture was stirred for 1 h, during which an orange precipitate and a light red solution formed. The mixture was reduced to dryness in vacuo, the residue was dissolved in 200 mL of THF, and the solution was filtered. The filtrate volume was reduced to ca. 125 mL, at which point an orange precipitate began to form. Ether (100 mL) was added, and the mixture was maintained at −20 °C overnight. The solid was collected by filtration, washed with acetonitrile (2 × 5 mL) and ether (2 × 5 mL), and dried in vacuo to afford the product as 0.550 g (69%) of an orange solid. The product can be recrystallized from dichloromethane/ether for an analytical sample. IR (KBr): ν_{SiO} 924 cm^{-1} (br), ν_{MoO} 920 or 895 cm^{-1}. Absorption data (CH_2Cl_2): λ_{max} (ϵ_M) 272 (28 100), 295 (sh, 15 000), 315 (sh, 8840), 426 (370) nm. ^1H NMR

(13) Holm, R. H. *Coord. Chem. Rev.* **1990**, *100*, 183.
(14) Enemark, J. H.; Young, C. G. *Adv. Inorg. Chem.* **1994**, *40*, 1.
(15) This group is commonly encountered in $[MoO_nS_{4-n}]^{2-}$ (n = 1−3), $[(R_2NO)_2MoOS]^{2-}$, and related tetrahedral species with four-electron ligands, examples of which have been structurally characterized.[16−20]
(16) Krebs, B.; Müller, A.; Kindler, E. *Z. Naturforsch.* **1970**, *25B*, 222.
(17) Kutzler, F. W.; Scott, R. A.; Berg, J. M.; Hodgson, K. O.; Doniach, S.; Cramer, S. P.; Chang, C. H. *J. Am. Chem. Soc.* **1981**, *103*, 6083.
(18) Wieghardt, K.; Hahn, M.; Weiss, J.; Swiridoff, W. *Z. Anorg. Allg. Chem.* **1982**, *492*, 164.
(19) Bristow, S.; Collison, D.; Garner, C. D.; Clegg, W. *J. Chem. Soc., Dalton Trans.* **1983**, 2495.
(20) Coucouvanis, D.; Toupadakis, A.; Lane, J. D.; Koo, S. M.; Kim, C. G.; Hadjikyriacou, A. *J. Am. Chem. Soc.* **1991**, *113*, 5271.
(21) Singh, R.; Spence, J. T.; George, G. N.; Cramer, S. P. *Inorg. Chem.* **1989**, *28*, 8. N_2S_2 is a tetradentate dianionic ligand.
(22) Romanenko, G. V.; Podberezskaya, N. V.; Fedin, V. P.; Geras'ko, O. A.; Fedorov, V. E.; Bakakin, V. V. *J. Struct. Chem.* **1988**, *29*, 79.
(23) Eagle, A. A.; Laughlin, L. J.; Young, C. G.; Tiekink, E. R. T. *J. Am. Chem. Soc.* **1992**, *114*, 9195. $HB(Me_2pz)_3$ = hydrotris(3,5-dimethylpyrazolyl)borate(1−).
(24) Young, C. G.; Laughlin, L. J.; Colmanet, S.; Scrofani, S. D. B. *Inorg. Chem.* **1996**, *35*, 5368.
(25) Faller, J. W.; Ma, Y. *Organometallics* **1989**, *8*, 609.
(26) Donahue, J. P.; Lorber, C.; Nordlander, E.; Holm, R. H. *J. Am. Chem. Soc.* **1998**, *120*, 3259.
(27) Donahue, J. P.; Goldsmith, C. R.; Nadiminti, U.; Holm, R. H. *J. Am. Chem. Soc.* **1998**, *120*, 12869.
(28) Lorber, C.; Donahue, J. P.; Goddard, C. A.; Nordlander, E.; Holm, R. H. *J. Am. Chem. Soc.* **1998**, *120*, 8102.
(29) Huang, M.; DeKock, C. W. *Inorg. Chem.* **1993**, *32*, 2287.
(30) Müller, A.; Dornfeld, H.; Schulze, H.; Sharma, R. C. *Z. Anorg. Allg. Chem.* **1980**, *468*, 193.

($CDCl_3$): δ 9.80, 9.10 (2 dd, 2,9-H), 8.14, 8.11 (dd, 4,7-H), 7.66, 7.63 (d, 5,6-H), 7.43 (m, 3,8-H). Anal. Calcd for $C_{48}H_{38}MoN_2O_3SSi_2$: C, 65.89; H, 4.38; Mo, 10.96; N, 3.20; S, 3.66. Found: C, 65.72; H, 4.43; Mo, 10.85; N, 3.16; S, 3.60.

[MoOS(OSiPh$_3$)$_2$(Me$_4$phen)]. A solution of 0.293 g (0.994 mmol) of Ph_3SiCl in 4 mL of acetonitrile was added dropwise to a stirred suspension of 0.134 g (0.527 mmol) of $K_2[MoO_3S]$ and 0.130 g (0.550 mmol) of Me_4phen in 5 mL of acetonitrile containing 1 mL of triethylamine. An orange precipitate and a red-brown solution formed. The mixture was stirred for 1 h, and the product was isolated by following the procedure in the previous preparation. The product was obtained as 0.202 g (41%) of an orange solid, which can be recrystallized from dichloromethane/ether. IR (KBr): ν_{SiO} 931 cm^{-1}, ν_{MoO} 920 or 901 cm^{-1}. Absorption data (CH_2Cl_2): λ_{max} (ϵ_M) 283 (29 000), 304 (sh, 10 000), 333 (1200), 434 (340) nm. ^{1}H NMR ($CDCl_3$): δ 9.58, 8.82 (2 s, 2,9-H), 7.84, 7.82 (2 d, 5,6-H), 2.57, 2.56, 2.34, 2.29 (4 s, 3,4,7,8-Me). Anal. Calcd for $C_{52}H_{46}MoN_2O_3SSi_2$: C, 67.08; H, 4.98; Mo, 10.30; N, 3.01; S, 3.44. Found: C, 66.92; H, 5.02; Mo, 10.37; N, 3.08; S, 3.46.

[MoOCl(OSiPh$_3$)$_2$(Me$_4$phen)]. A solution of 34.5 mg (0.037 mmol) of [MoOS(OSiPh$_3$)$_2$(Me$_4$phen)] in 2 mL of dichloromethane was treated with 9.70 mg (0.037 mmol) of PPh_3 in 0.5 mL of dichloromethane. The orange solution turned red within minutes; ether (40 mL) was added until precipitation occurred. The solid was collected by filtration and dried in vacuo, affording the product as 21.7 mg (63%) of a red solid. The compound may be further purified by recrystallization from THF/hexanes and obtained as red crystals. IR (KBr): ν_{SiO} 927 (s) cm^{-1}. Absorption data (CH_2Cl_2): λ_{max} (ϵ_M) 269 (sh, 23 900), 284 (23 900), 308 (sh, 11 100), 329 (sh, 4020), 382 (sh, 973), 407 (sh, 709), 504 (524) nm. FAB-MS: *m*/*z* 935 (M^+), 900 ($M^+ - Cl$). Anal. Calcd for $C_{52}H_{46}ClMoN_2O_3Si_2$: C, 66.83; H, 4.96; Cl, 3.79; Mo, 10.27; N, 3.00. Found: C, 67.04; H, 5.04; Cl, 3.85; Mo, 10.24; N, 2.88.

[MoO$_2$(OSiPh$_3$)$_2$(Me$_2$bpy)]. The same procedure was used for two compounds. A solution of 0.150 g (0.221 mmol) of [MoO$_2$(OSiPh$_3$)$_2$] in 4 mL of dichloromethane was treated with a solution of 0.049 g (0.265 mmol) of Me$_2$bpy (4,4′- or 5,5′-dimethyl-2,2′-bipyridine). After 10 min, the colorless solution was filtered and the filtrate was layered with 15 mL of ether. The product separated as colorless crystals, which were collected by filtration, washed with acetonitrile (4 × 5 mL) and ether (2 × 5 mL), and dried in vacuo.

(a) 4,4′-Me$_2$bpy. The product was collected as 0.162 g (85%). IR (KBr): 933 (vs, ν_{SiO}), 912, 901 (s, ν_{MoO}) cm^{-1}. Absorption spectrum (CH_2Cl_2): λ_{max} (ϵ_M) 254 (14100), 298 (sh, 9420), 308 (10300) nm. FAB-MS: *m*/*z* 864 (M^+), 848 (M^+-O). ^{1}H NMR ($CDCl_3$): δ 8.94 (d, 1), 7.22 (m, 9), 7.09 (m, 6), 7.03 (s, 1), 6.93 (d, 1), 2.32 (s, 3). Anal. Calcd for $C_{48}H_{42}MoN_2O_4Si_2$: C, 66.81; H, 4.91; Mo, 11.12; N, 3.25. Found: C, 66.67; H, 4.91; Mo, 11.06; N, 3.32.

(b) 5,5′-Me$_2$bpy. The product was collected as 0.146 g (76%). Absorption data (CH_2Cl_2): λ_{max} (ϵ_M) 258 (12 600), 319 (8950) nm. FAB-MS: *m*/*z* 864 (M^+), 848 ($M^+ - O$). IR (KBr): 945 (vs, ν_{SiO}), 908 (s, ν_{MoO}) cm^{-1}. ^{1}H NMR ($CDCl_3$): δ 8.83 (s, 1), 7.41 (d, 1), 7.30 (d, 1), 7.22 (m, 9), 7.10 (m, 6), 2.18 (s, 3). Anal. Found: C, 66.90; H, 4.86; Mo, 11.22; N, 3.21.

[MoO$_2$(OSiPh$_3$)$_2$(py)$_2$]. A solution of 0.050 g (0.074 mmol) of [MoO$_2$(OSiPh$_3$)$_2$] in 1 mL of dichloromethane was treated with 10 drops of pyridine. After 10 min of stirring, the colorless solution was filtered and the filtrate was layered with 4 mL of ether, causing precipitation of a colorless crystalline solid. This material was collected by filtration, washed with 2 × 5 mL of ether, and dried in vacuo to afford the product as 0.066 g (89%) of colorless crystals. Absorption data (CH_2Cl_2): λ_{max} (ϵ_M) 257 (7260) nm. IR (KBr): 903 (br, s). ^{1}H NMR ($CDCl_3$): δ 8.68 (d, 2), 8.03 (t, 1), 7.64 (d, 6), 7.59 (t, 2), 7.38−7.44 (m, 9). Anal. Calcd for $C_{46}H_{40}MoN_2O_4Si_2$: C, 66.01; H, 4.82; Mo, 11.46; N, 3.35. Found: C, 65.88; H, 4.76; Mo, 11.42; N, 3.28.

[MoOS(OSiPh$_3$)$_2$(Me$_2$bpy)]. The same procedure was used for two compounds. A suspension of 0.200 g (0.787 mmol) of $K_2[MoO_3S]$ in 5 mL of acetonitrile containing 0.5 mL of triethylamine was treated with 0.261 g (1.42 mmol) of Me$_2$bpy. To this mixture was added a solution of 0.441 g (1.50 mmol) of Ph_3SiCl in 5 mL of acetonitrile, resulting in the appearance of a red-brown solution within 10 s and an orange precipitate within 1 min. The mixture was stirred for at least 2 h. The solid was collected by filtration, washed with acetonitrile (4 × 5 mL), and redissolved in 5 mL of dichloromethane, and the mixture was filtered to remove KCl. The product was isolated by immediate volume reduction of the filtrate in vacuo to minimize decomposition that slowly occurs in solution.

Chart 1. Designation of Molybdenum Complexes

[MoO$_2$(OSiPh$_3$)$_2$(phen)]	**1**
[MoO$_2$(OSiPh$_3$)$_2$(Me$_4$phen)]	**2**
[MoO$_2$(OSiPh$_3$)$_2$(4,4′-Me$_2$bpy)]	**3**
[MoO$_2$(OSiPh$_3$)$_2$(5,5′-Me$_2$bpy)]	**4**
[MoO$_2$(OSiPh$_3$)$_2$(py)$_2$]	**5**
[MoOS(OSiPh$_3$)$_2$(phen)]	**6**
[MoOS(OSiPh$_3$)$_2$(Me$_4$phen)]	**7**
[MoOS(OSiPh$_3$)$_2$(4,4′-Me$_2$bpy)]	**8**
[MoOS(OSiPh$_3$)$_2$(5,5′-Me$_2$bpy)]	**9**
[MoOCl(OSiPh$_3$)$_2$(Me$_4$phen)]	**10**

(a) 4,4′-Me$_2$bpy. The product was collected as 0.247 g (36%) of an orange solid. Absorption data (CH_2Cl_2): λ_{max} (ϵ_M) 250 (sh, 27 900), 303 (sh, 20 200), 310 (21 200), 424 (486) nm. IR (KBr): 924 (vs, ν_{SiO}), 908 (sh, ν_{MoO}) cm^{-1}. FAB-MS: *m*/*z* 880 (M^+), 864 ($M^+ - O$), 848 ($M^+ - S$). ^{1}H NMR ($CDCl_3$): δ 9.49 (d, 1), 8.74 (d, 1), 7.23 (m, 18), 7.17 (s, 2), 7.11 (m, 12), 6.93 (dd, 2), 2.36 (s, 6). Anal. Calcd for $C_{48}H_{42}MoN_2O_3SSi_2$: C, 65.58; H, 4.82; Mo, 10.91; N, 3.19; S, 3.65. Found: C, 65.75; H, 4.82; Mo, 10.73; N, 3.25; S, 3.85.

(b) 5,5′-Me$_2$bpy. The product was collected as 0.345 g (50%) of an orange solid. Absorption data (CH_2Cl_2): λ_{max} (ϵ_M) 252 (16 400), 318 (12 500), 424 (464) nm. IR (KBr): 924 (vs, ν_{SiO}), 908, (sh, ν_{MoO}) cm^{-1}. FAB-MS: *m*/*z* 880 (M^+), 864 ($M^+ - O$), 848 ($M^+ - S$). ^{1}H NMR ($CDCl_3$): δ 9.33 (s, 1), 8.64 (s, 1), 7.43 (m, 4), 7.23 (m, 18), 7.11 (m, 12), 2.23 (s, 3), 2.21 (s, 3). Anal. Found: C, 65.39; H, 4.93; Mo, 10.97; N, 3.26; S, 3.54.

In the sections that follow, complexes are designated according to Chart 1.

X-ray Structure Determinations. Crystallizations were conducted anaerobically. Crystals of **1** (clear plates) and of **6** and **7** (orange blocks) were grown by vapor diffusion of ether into dichloromethane solutions. For the last two compounds, rigorously dry conditions were used. Crystals of **5** (clear blocks) were grown by slow evaporation of an acetonitrile solution. Crystals of **10** (red needles) were obtained by slow diffusion of cyclohexane into a THF solution. Crystals were coated in oil and mounted on a Siemens (Bruker) CCD area detector instrument operated by the SMART software package. Data were collected at 213 K and were measured by using ω scans of 0.3° per frame, with 30 or 60 s frames, such that 1271 frames were collected for a hemisphere of data. The first 50 frames were recollected at the end of the data collection to monitor for decay; no appreciable decay was detected for any compound. For **1**, data were used only out to 2θ of 45° owing to the weakness of higher angle reflections, but for **6** and **7**, all data out to 2θ of 56° were used, allowing for a final resolution of 0.76 Å. For **10**, data extended to 2θ of 50°. Cell parameters were retrieved using SMART software and refined using SAINT software on all observed reflections between 2θ of 3° and the indicated upper thresholds. Data reduction was performed with SAINT, which corrects for Lorentz−polarization and decay effects. Absorption corrections were applied using SADABS, as described by Blessing.[31] For compounds **1**, **5**, **6**, and **7**, analysis of systematic absences by the program XPREP identified the space group as either *Cc* or *C*2/*c*. The latter was chosen over the former in all four cases on the basis of successful structure solution and refinement. The space group of **10** was unambiguously identified as $P2_1/c$ by systematic absences using XPREP. Crystal parameters are collected in Tables 1 and 2.

(31) Blessing, R. H. *Acta Crystallogr.* **1995**, *A51*, 33.

Table 1. Crystallographic Data[a] for $[MoO_2(OSiPh_3)_2(phen)]$ (**1**), $[MoO_2(OSiPh_3)_2(py)_2]$ (**5**), $[MoOS(OSiPh_3)_2(phen)]$ (**6**), $[MoOS(OSiPh_3)_2(Me_4phen)]$ (**7**), and $[MoOCl(OSiPh_3)_2(Me_4phen)]\cdot C_6H_{12}$ (**10**·C_6H_{12})

	1	**5**	**6**	**7**	**10**·C_6H_{12}
formula	$C_{48}H_{38}MoN_2O_4Si_2$	$C_{46}H_{40}MoN_2O_4Si_2$	$C_{48}H_{38}MoN_2O_3SSi_2$	$C_{52}H_{46}MoN_2O_3SSi_2$	$C_{58}H_{58}ClMoN_2O_3Si_2$
fw	858.92	836.92	874.98	931.09	1018.63
crystal system	monoclinic	monoclinic	monoclinic	monoclinic	monoclinic
space group	*C2/c*	*C2/c*	*C2/c*	*C2/c*	$P2_1/c$
Z	4	4	4	4	4
a, Å	15.686(2)	10.0939(2)	15.7695(6)	16.7020(8)	19.0483(9)
b, Å	9.758(1)	15.8957(4)	9.7836(3)	10.3747(5)	14.4601(7)
c, Å	27.442(3)	25.8051(7)	27.7370(2)	27.039(1)	18.1676(8)
β, deg	105.033(3)	98.056(1)	103.714(2)	103.472(1)	90.576(2)
V, Å^3	4056.7(9)	4099.6(2)	4157.3(2)	4556.3(4)	5003.8(4)
R_1,[b] wR_2[c]	0.0503, 0.0755	0.0339, 0.0755	0.0411, 0.1028	0.0430, 0.0884	0.0658, 0.1148

[a] Obtained with graphite-monochromatized Mo Kα ($\lambda = 0.710\ 73$ Å) radiation at $T = 213$ K. [b] $R_1 = \sum||F_o| - |F_c||/\sum|F_o|$. [c] $wR_2 = \{\sum[w(F_o^2 - F_c^2)^2]/\sum[w(F_o^2)^2]\}^{1/2}$.

Table 2. Selected Interatomic Distances (Å) and Angles (deg) for $Mo^{VI}O_2$ (**1**, **5**) and $Mo^{VI/V}OX$[a] (**6**, **7**, **10**) Complexes

	1	**5**	**6**[g]	**7**[g]	**10**·C_6H_{12}
Mo−O_{oxo}[b]	1.70(1)	1.695(2)	1.611(5)	1.645(5)	1.703(4)
Mo−X[a]			2.257(3)	2.203(2)	2.424(2)
Mo−O_{Si}[c]	1.92(1)	1.931(1)	1.923(2)	1.932(2)	1.935(8)[f]
Mo−N_O[d]	2.34(1)	2.404(4)	2.445(4)	2.41(2)	2.297(4)
Mo−N_S[d]			2.194(3)	2.28(2)	
Si−O	1.61(1)	1.601(1)	1.595(2)	1.618(2)	1.622(4)
O_{oxo}−Mo−O_{oxo}'[b]	106.5(9)	104.5(1)			
O_{oxo}−Mo−X[a]			103.3(2)	104.6(2)	95.4(1)
O_{oxo}−Mo−O_{Si}	98.0(5)	98.65(7)	101.8(2)	100.7(3)	105.9(4)[f]
X−Mo−O_{Si}[a]			95.84(9)	99.56(9)	86.9(1)[h]
O_{Si}−Mo−O_{Si}'[c]	153.1(6)	151.7(9)	153.0(1)	154.1(1)	90.8(2)
O_{oxo}−Mo−N[e]	91.8(6)	90.2(1)	97.0(2)	96.3(7)	88.3(2)
O_{oxo}−Mo−N′[e]	161.7(6)	165.3(1)	167.1(2)	168.2(7)	159.5(2)
X−Mo−N[a,e]			159.7(1)	158.5(6)	87.2(1)
X−Mo−N′[a,e]			89.6(1)	87.2(6)	80.6(1)
O_{Si}−Mo−N[e]	80.0(4)	78.8(1)	80.4(1)	81.2(7)	89.4(2)[h]
O_{Si}−Mo−N′[e]	78.0(4)	78.9(1)	77.7(1)	77.8(7)	86.0(4)[f]
N−Mo−N′[e]	70.0(9)	75.1(2)	70.1(2)	72(1)	71.5(2)
Mo−O−Si	160.4(6)	146.3(1)	157.8(1)	153.1(1)	156.6(5)[f]

[a] X = S, Cl. [b] O_{oxo} = O(1), O_{oxo}' = O(1′). [c] O_{Si} = O(2, 3), O_{Si}' = O(2′, 4). [d] N_O, N_S = trans to O_{oxo}, S. [e] N = N(1), N′ = N(1′, 2). [f] Mean values. [g] Disordered structures; see text. [h] Trans Cl−Mo−O_{Si} = 161.8(1)°, trans O_{Si}-Mo−N = 161.9(2)°.

All structures were solved by direct methods with SHELXS and subsequently refined against all data in the 2θ ranges by full-matrix least-squares calculations based on F^2. In the structures of **6** and **7**, the oxo and sulfido ligands as well as the phen and Me_4phen ligands were disordered and refined with site occupancy factors of 0.5 for all atoms. The Ph_3SiO ligands in these two compounds were also disordered between two rotational configurations, which were modeled with site occupancy factors determined as optimal fits by SHELXL. In the structure of **5**, a pyridine and three phenyl rings were disordered equally over two positions. All non-hydrogen atoms were refined anisotropically, including those which are disordered. The carbon atoms of the phen and Me_4phen ligands in **6** and **7** and a pyridine ligand in **5**, although refined anisotropically, required the use of averaged thermal parameters to maintain reasonably sized ellipsoids in structure presentations. Hydrogen atoms were attached at idealized positions on carbon atoms and were refined as riding atoms with uniform values of U_{iso}. All structures converged in the final stages of refinement, showing no movement in atom positions and no residual electron density >1 e/Å^3. Bond distances and angles were not constrained in refinements, except for the two N-containing rings of the phen ligand in **6** and the pyridine ring of **5** which were constrained to regular hexagons. Because of disorder, data from two crystals of **6** obtained from independent preparations were collected and fully refined. Values of all bond distances and angles involving the molybdenum atom agreed to within 4σ. Results for the refinement with the marginally better *R* values are reported. Use of the checking program PLATON did not identify any missing or higher symmetry. Final agreement factors are given in Table 1.[32]

X-ray Absorption Spectroscopy. Solid samples of complexes **1** and **6**−**9** were ground into fine powders in a dinitrogen atmosphere and diluted with boron nitride. The mixtures were pressed into pellets and sealed between 63.5 μm Mylar tape windows in a 1 mm aluminum spacer. The samples were frozen in liquid nitrogen immediately upon removal from the glovebox and maintained at this or a lower temperature throughout storage and data collection.

(a) Data Collection. XAS data were measured at the Stanford Synchrotron Radiation Laboratory (SSRL) on unfocused 8-pole wiggler beamline 7-3 under ring conditions of 3.0 GeV and 70−100 mA. A Si(220) double-crystal monochromator was used and detuned 50% at 21549 eV to minimize contamination from higher harmonics. An Oxford Instruments CF1208 continuous-flow liquid helium cryostat maintained a constant sample temperature of 10 K. Data were measured in the transmission mode to $k = 20$ Å^{-1} with argon as the absorbing gas. Internal calibration was performed by simultaneous measurement of the absorption edge of a molybdenum foil placed between a second and a third ionization chamber. The first inflection point of the foil spectrum was assigned to 20 003.9 eV. The data represent averages of two or three scans for each sample with data reduction as described previously in detail.[33]

(b) Data Analysis. The data analysis was performed using the ab initio GNXAS method. The theoretical basis for the GNXAS approach and its fitting methodologies have been described in detail elsewhere.[34−36] The program code generates theoretical EXAFS signals on the basis of an initial structural model. For the analysis reported here, the crystallographic coordinates for complexes **1**, **6**, and **7** were used to generate an initial structural model up to a distance cutoff of 5.0 Å. For complexes **8** and **9**, modifications were made to the crystal structure of **6** (utilizing Chem3D Pro) to replace the phenanthroline ligand with that of a known bipyridine structure and generate new coordinates. Phase shifts were obtained using the standard muffin-tin approximation to calculate the individual two-body and three-body EXAFS signals. An initial model EXAFS spectrum was constructed by combining the individual component signals and an appropriate background. This model was then fit to the averaged raw absorption data by a least-squares minimization program as described previously.[36] If any of the distances determined in the fits differed by more than 10% from those in the initial starting model, the phase and amplitude parameters were recalculated after modification of the model bond lengths using

(32) See also paragraph at the end of paper regarding Supporting Information.
(33) DeWitt, J. G.; Bentsen, J. G.; Rosenzweig, A. C.; Hedman, B.; Green, J.; Pilkington, S.; Papaefthymiou, G. C.; Dalton, H.; Hodgson, K. O.; Lippard, S. J. *J. Am. Chem. Soc.* **1991**, *113*, 9219.
(34) Filipponi, A.; Di Cicco, A.; Tyson, T. A.; Natoli, C. R. *Solid State Commun.* **1991**, *78*, 265.
(35) Westre, T. E.; Di Cicco, A.; Filipponi, A.; Natoli, C. R.; Hedman, B.; Solomon, E. I.; Hodgson, K. O. *J. Am. Chem. Soc.* **1995**, *117*, 1566.
(36) Filipponi, A.; Di Cicco, A.; Natoli, C. R. *Phys. Rev. B* **1995**, *52*, 15122, 15135.

Chem3D Pro. Background subtraction was performed by applying a flexible three-segment spline which was refined in the GNXAS fits. The quality of the fit was calculated by the least-squares residual R and monitored through visual inspection of the fits to the data and Fourier transform (FT), the residual EXAFS signal, and its Fourier transform. The structural parameters varied during the refinements were the bond distance (R) and the bond variance (σ_R^2)[36] in the case of a two-body signal, the two shorter bond distances R_1 and R_2, the intervening angle (θ), and the six covariance matrix elements for a three-body signal. The nonstructural parameters E_o and S_o^2 were varied, whereas the Γ_C (core hole lifetime) and E_r (experimental resolution) were kept fixed to physically reasonable values throughout the analysis. The coordination numbers were initially set to the values determined by X-ray crystallography for structures **1**, **6**, and **7** (complexes **8** and **9** were assumed to have the same coordination numbers as **6** and **7**) and were then systematically stepped through during the analysis as necessary. All parameters were varied within a preset range, and all results were checked to ensure that values obtained did not reach the high or low point of these fitting ranges.

Results and Discussion

At least three synthetic routes to five- or six-coordinate complexes containing the *cis*-$Mo^{VI}OS$ group are evident: (i) replacement of oxo by sulfido in a $Mo^{VI}O_2$ complex; (ii) oxidative addition of S(0) to an $Mo^{IV}O$ complex and/or O(0) to an $Mo^{IV}S$ complex; (iii) derivatization of a species containing an $Mo^{VI}OS$ fragment. While route i has been accomplished in the reaction $[(R_2NO)_2MoO_2]^{2-} \rightarrow [(R_2NO)_2MoOS]^{2-}$ with H_2S[18] or B_2S_3,[19] a similarly direct conversion has not been successfully applied to molecules having only two four-electron ligands. In a variation of this route, $[(HB(Me_2pz)_3)Mo^{VI}O_2(\eta^1\text{-}S_2PR_2)]$ was reduced to the $Mo^{V}O_2$ state, one oxo group was substituted by reaction with hydrosulfide, and the resultant species was oxidized to $[(HB(Me_2pz)_3)Mo^{VI}OS(\eta^1\text{-}S_2PR_2)]$.[37] Both procedures of route ii have yielded the latter complexes.[23,24] In our approach, we utilized route iii in a manner suggested by two prior observations. Treatment of Ag_2MoO_4 with Ph_3SiCl affords tetrahedral $[MoO_2(OSiPh_3)_2]$ in >90% yield.[29] The coordinative unsaturation of this species is made evident by the reaction with Ph_3P to give $[MoO_2(OSiPh_3)_2(PPh_3)]$.[29] These findings are capable of extension in the form of the reactions in Figure 2.

$Mo^{VI}O_2$ Complexes. (a) Synthesis and Properties. Assessment of the properties of $Mo^{VI}OS$ species requires the corresponding dioxo complexes as references, particularly because they are not subject to the same potential disorder problem in the crystalline state. Initially, $[MoO_2(OSiPh_3)_2]$[29] was reacted with phen, bpy, or py ligands to form the colorless dioxo complexes **1**-**5**, which are readily isolated in 74−96% yields. These species show intense ν_{SiO} and ν_{MoO} stretches (when observable) in the 890−945 cm^{-1} region and prominent parent ion peaks in the FAB mass spectra (**3**, **4**). They display ^1H NMR spectra indicative of C_2 symmetry with deshielded 2,9-H (**1**, **2**) and 6,6′-H (**3**, **4**) resonances at δ 8.8−9.3; the related pyridine α-H signal of **5** occurs at δ 8.38. This effect is illustrated by the spectra of **1** and **4** in Figure 3, where the 2,9-H (doublet of doublets) and 6,6′-H (broadened singlet) signals appear at δ 9.28 and 8.83, respectively.

(b) X-ray Structures. The X-ray structures of **1** and **5** are presented in Figure 4; selected metric data are compiled in Table 2. These compounds crystallize in monoclinic space group $C2/c$; the asymmetric unit consists of one half the molecule, with the other half generated by a C_2 axis that bisects the O−Mo−O and N−Mo−N angles. Given the structure of **5**, the chelate ring plays no role in setting the overall stereochemistry.

(37) Laughlin, L. J.; Young, C. G. *Inorg. Chem.* **1996**, *35*, 1050.

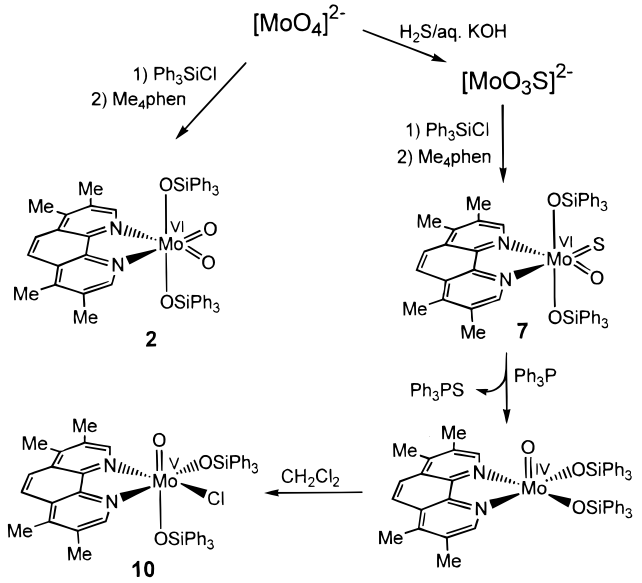

Figure 2. Preparation of Me_4phen complexes **2**, **7**, and **10**. Reactions affording $Mo^{VI}O_2$ complexes **1** and **3**−**5** and $Mo^{VI}OS$ complexes **6**, **8**, and **9** are analogous. The $Mo^{IV}O$ species is a proposed intermediate in the reduction of **7** by oxo transfer.

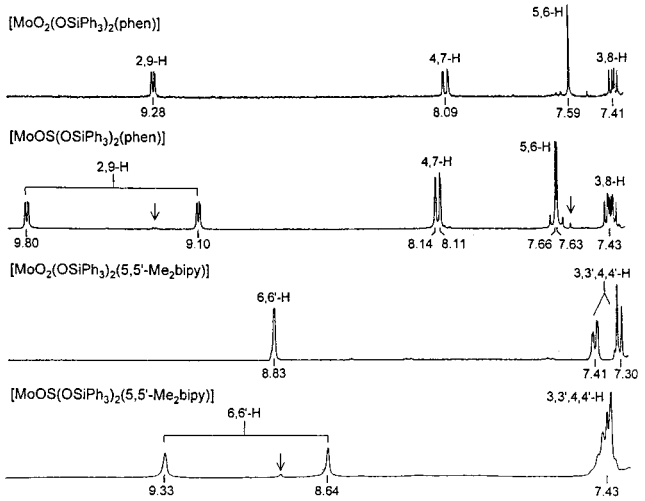

Figure 3. ^1H NMR spectra of $[MoO_2(OSiPh_3)_2(phen)]$, $[MoOS(OSiPh_3)_2(phen)]$, $[MoO_2(OSiPh_3)_2(5,5'\text{-}Me_2bpy)]$, and $[MoOS(OSiPh_3)_2(5,5'\text{-}Me_2bpy)]$ in $CDCl_3$ solutions, emphasizing the absence of C_2 symmetry in the $Mo^{VI}OS$ complexes. Chemical shifts are indicated; arrows in two spectra mark trace impurities of dioxo complexes.

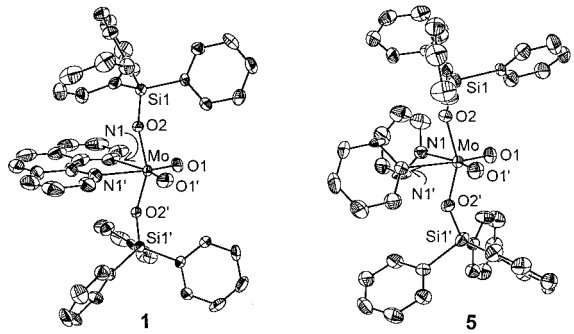

Figure 4. Structures of $[MoO_2(OSiPh_3)_2(phen)]$ (**1**) and $[MoO_2(OSiPh_3)_2(py)_2]$ (**5**), showing 50% probability ellipsoids and atom-labeling schemes. Primed and unprimed atoms are related by a 2-fold axis.

Indeed, these two complexes (and, by implication, **2**−**4**) exhibit the conventional stereochemistry of $[Mo^{VI}O_2L_2L'_2]$ molecules, in which anionic ligands L′ are mutually trans and cis to oxo

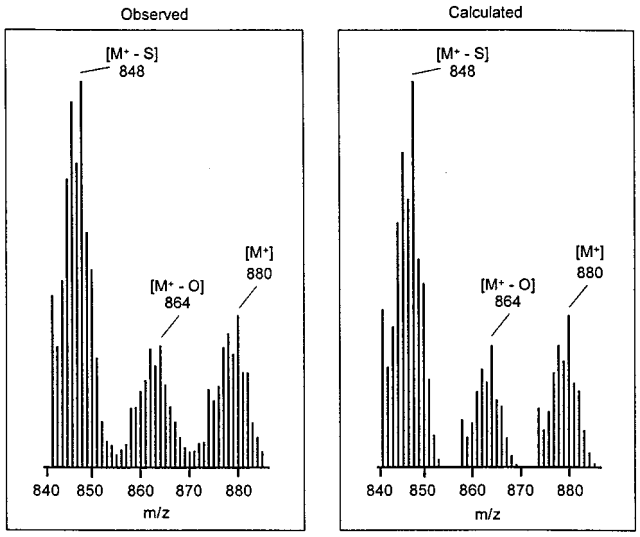

Figure 5. FAB$^+$ mass spectrum of [$MoOS(OSiPh_3)_2$(4,4′-Me_2bpy)] and the calculated spectrum in the parent ion region.

and neutral ligands L. Dimensions of the MoO_2 group are essentially identical and are normal. Owing to charge repulsion, the silyloxy groups are bent back from the oxo ligands, causing O−Mo−O bond angles of 152−154°. The Mo−O−Si fragments are also nonlinear (146−160°), as in [$MoO_2(OSiPh_3)_2$][29] and other molybdenum complexes.[27] The Mo−O−Si angles open toward the MoO_2 group, and in **1** and **5**, the Mo−O−Si plane exactly bisects the MoO_2 angle. Because in **5** the pyridine rings are rotated out of the Mo(O1)(O1′) plane (dihedral angle 68.7°), the smaller Mo−O−Si angle (146.3(1)°) serves to reduce steric interactions between the pyridine rings and the $SiPh_3$ groups.

$Mo^{VI}OS$ Complexes. (a) Synthesis and Properties. Heterogeneous reaction of $K_2[MoO_3S]$, Ph_3SiCl, and phen or bpy in acetonitrile results in the formation of the desired complexes **6**−**9** in 36−69% yields as orange solids (Figure 2). Compound identification is based on elemental analyses, mass spectra (**8**, **9**), ^{1}H NMR spectra, X-ray structure determinations (**6**, **7**), and molybdenum K-edge EXAFS analyses. All compounds show the correct sulfur content, indicating no appreciable contamination with dioxo species. The mass spectra of **8** in Figure 5 and of **9** (not shown) reveal in the high *m*/*z* region the parent ion and two fragments resulting from the loss of one oxygen or sulfur atom. The NMR spectra of **6** and **9** in Figure 3 disclose unsymmetrically coordinated phen and 5,5′-Me_2bpy ligands, indicative of the absence of C_2 symmetry present in dioxo counterparts **1** and **4**. Complexes **7** (0.76) and **8** (0.75) show the same behavior with the indicated chemical shift differences (ppm) between the 2,9-H and 6,6′-H signals, respectively. The orange color of the four complexes arises from absorption bands at 424−434 nm shown in Figure 6. These features are absent in the dioxo complexes and arise, therefore, from S → Mo charge transfer. The intensity of these bands ($\epsilon_M \approx 400-500$) is sufficiently low that they would be obscured by other chromophores (flavins, iron−sulfur clusters) that occur in the xanthine oxidase enzyme family.

(b) X-ray Structures. Complexes **6** and **7** also crystallize in space group *C*2/*c*; the unit cells of **1** and **6** are nearly isometric. Structures are presented in Figure 7, from which it is evident that these molecules possess the same overall stereochemistry as the dioxo species. The imposed C_2 symmetry at the molybdenum special position requires that the crystal contain a 1:1 mixture of identical molecules distinguished only by the relative orientation of the *cis*-$Mo^{VI}OS$ group. Fortuitously, the

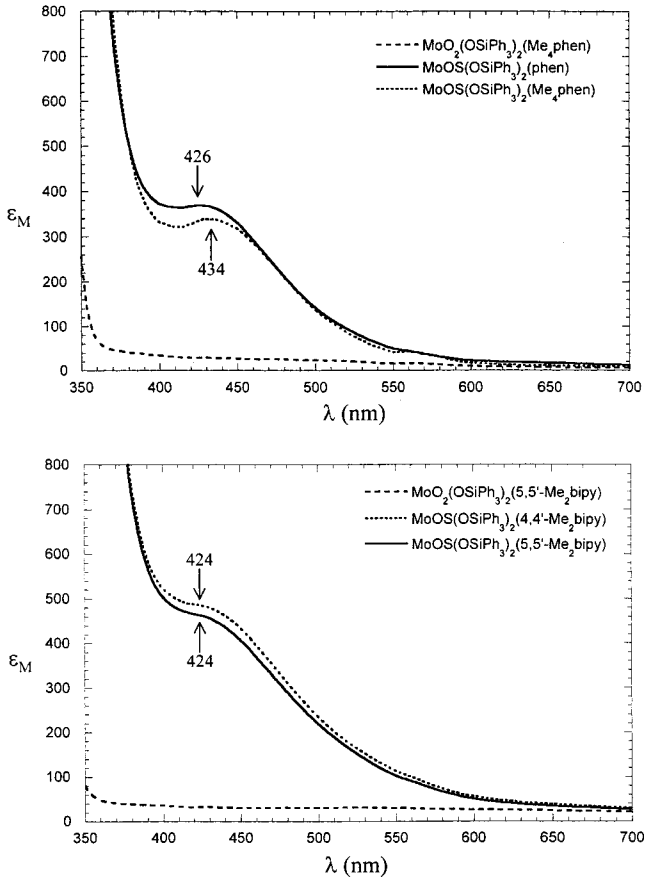

Figure 6. Absorption spectra of $Mo^{VI}O_2$ and $Mo^{VI}OS$ complexes in dichloromethane solutions. Band maxima are indicated.

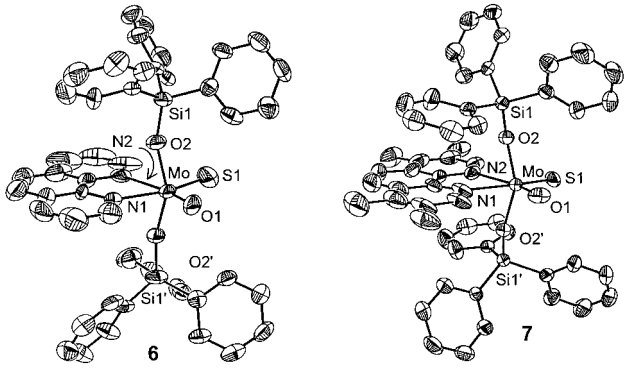

Figure 7. Structures of [$MoOS(OSiPh_3)_2$(phen)] (**6**) and [$MoOS(OSiPh_3)_2(Me_4phen)$] (**7**) showing 50% probability ellipsoids and atom-labeling schemes. Primed and unprimed atoms are related by a 2-fold axis.

oxo and sulfido ligands are not symmetrically disposed on either side of the C_2 axis, such that when the symmetry-equivalent atoms (O′, S′) are generated, they do not overlap the original atoms. Thus the atoms O, S, O′, S′ are four separate resolved peaks in the electron density maps, which were refined anisotropically as atoms of half-site occupancy. The presence of the *cis*-$Mo^{VI}OS$ group requires that the phen and Me_4phen ligands be unsymmetrically coordinated. In both cases, the Mo−N distance trans to the oxo ligand (Mo−N_O) is apparently lengthened by ca. 0.2 Å compared to the Mo−N distance trans to the sulfido ligand (Mo−N_S) (Table 2). This skewed ligand binding coupled with the presence of the C_2 axis necessitates that the phen and Me_4phen ligands be disordered between two highly overlapping positional variants. All carbon atoms of these disordered ligands are discernible in electron density maps. They

were refined anisotropically as atoms with half-site occupancies and averaged thermal parameters. Bond distances and angles for **6** and **7** refined as described are contained in Table 2.

The foregoing evidence collectively demonstrates the presence of the *cis*-$Mo^{VI}OS$ group in complexes **6**−**9**, albeit with apparent differences in certain metric parameters as obtained by the refinement procedure: Mo═O 1.607(5) (**6**), 1.645(5) (**7**) Å; Mo═S 2.257(3) (**6**), 2.203(2) (**7**) Å. The Mo═O distances are 0.05−0.09 Å shorter than the values in the dioxo complexes (Table 2). The Mo═S bond lengths are also somewhat long when compared to tetrahedral Mo^{VI}═S bonds (2.10−2.18 Å),[16−20,38] consistent with the few six-coordinate values available, viz. for $[MoOSCl_2(OPPh_3)_2]$[22] and $[(HB(Me_2pz)_3)MoOS(\eta^1\text{-}S_2PR_2)]$.[23] In both structures, the closest intermolecular and nonbonded intramolecular distances are not less than 2.70 Å and involve hydrogen atoms; consequently, the $Mo^{VI}OS$ group is unperturbed. The Mo−N_O/N_S bond distances differ by 0.27 Å in **5** and 0.14 Å in **6**. The longer distances are for bonds trans to the oxo ligands. The formation of a relatively short and strong Mo−N_S bond leads to a longer and weaker Mo−N_O bond. The effect arises at least in part because of the rigidity and small bite angle (ca. 70°) of the phen ligands, which prevent expression of the intrinsic trans influence of oxo and sulfido ligands in bonds disposed at or near 90°.[39] Note that, in $[(HB(Me_2pz)_3)MoOS(\eta^1\text{-}S_2PR_2)]$ (0.10 Å)[23] and $[(HB(Me_2pz)_3)W^{VI}OS((-)\text{-mentholate})]$ (0.05 Å),[40] where the tridentate ligand is more flexible, and in $[W^{VI}OS(NCS)_4]^{2-}$ (0.02 Å),[41] the differential O/S trans influence on M−N bonds, as expressed by bond length differences, is much less. The distorted square pyramidal $[Mo^{VI}OS(S_2pd)(OH_2)]$ site of *D. gigas* aldehyde oxidoreductase places the sulfido ligand in the axial position and the remaining ligands in the equatorial plane.[7] Structural resolution is insufficient to detect any oxo trans influence on dithiolene binding.

Terminal oxo−sulfido ligand disorder is well documented and has been manifested in different modes: within nonlinear[25,42,43] and linear[44] MOS groups, over the sites of two different metals in the same molecule,[45,46] and in the formation of solid solutions[47,48] (as with $(Me_4N)_2[MoS_3Q]$ (Q = O, S)[48]). Potential disorder is sometimes circumvented by differentiating interactions, such as the intramolecular effect Mo═S···S═P in the molecular lattice of $[(HB(Me_2pz)_3)MoOS(\eta^1\text{-}S_2PPr^i_2)]$[23] and cation−anion interactions in the ionic lattice of $(NH_4)_2[WO_2S_2]$.[49] Relatively large molecules with pseudo-2-fold symmetry, in which the MOS group is shielded from the crystalline environment and any attendant differentiating interactions, are favorable cases for disorder. That is the condition of **6** and **7**, in which protruding phenyl rings provide frontside hindrance to the $Mo^{VI}OS$ group. While the existence of this group in **6**−**9** is not in question, the accuracy of its bond lengths is uncertain, especially when the differences in the Mo═O and Mo═S distances are comparable to the resolution of the X-ray experiment ($\lambda/(2\sin\theta_{max}) \approx 0.5$ Å). Any uncertainties in these distances would not appear to arise from dioxo contamination, which would have the effect of moving together overlapping electron densities. If Mo═O = 1.70 Å from dioxo structures is adopted, the presence of the $Mo^{VI}O_2$ group would lengthen the Mo═O and contract the Mo═S distance. To obtain metric parameters of the $Mo^{VI}OS$ group uncomplicated by disorder, we utilized X-ray absorption spectroscopy.

XAS Spectroscopy. Five complexes were examined, one of the $Mo^{VI}O_2$ type (**1**) and the four $Mo^{VI}OS$ species (**6**−**9**). Fit parameters and derived bond distances and angles are compiled in Table 3. Relevant spectra are presented in Figures 8−11.

(a) EXAFS Analysis. The EXAFS data and Fourier transforms of complexes **6** and **7** are essentially superimposable to the end of the high-k range (20 $Å^{-1}$), as are those of **8** and **9**. It therefore suffices to focus on the results for $Mo^{VI}O_2$ complex **1** and $Mo^{VI}OS$ complexes **7** and **9**. As shown in Figure 8, there are significant differences in the EXAFS beat patterns, particularly in the $k \sim 7$ and $k \sim 13$ $Å^{-1}$ regions for **1** as compared to **7** and **9**. This is also reflected in the Fourier transforms in Figure 9, where it is seen that the intensities of all peaks of **1** differ from those of **7** and **9**, which themselves are quite similar. The intensity of the first peak of **1**, which corresponds to Mo═O interactions, has increased significantly relative to those of the other two complexes, in agreement with the presence of two oxo ligands. The second and third peaks have lower intensities for **1**, an effect attributable to the absence of Mo═S ligation. For complex **1**, the second and third peaks represent Mo−O and Mo−N interactions, respectively. In addition to these contributions, the Mo═S interaction present in **7** and **9** contributes substantially to the intensities of both the second and third peaks. Sulfur is a very strong backscatterer, and its presence often dominates, especially in molecules with weak scattering ligands such as oxygen and nitrogen.

For complex **1**, the EXAFS fit results are in outstanding agreement with the crystal structure (Table 2), with single-scattering contributions from two Mo═O, two Mo−O, and two Mo−N distances at 1.72, 1.94, and 2.36 Å, respectively. Excellent fits to the data for **6** and **7** were achieved by including only single-scattering interactions. The results indicate the presence of one short Mo═O distance of 1.71−1.72 Å, two longer Mo−O distances of 1.95 Å, a short Mo═S distance of 2.19 Å, and two longer Mo−N interactions at a distance of 2.37 Å. The possibility of a split outer Mo−N shell, as indicated in the X-ray work, was tested in further refinements but did not lead to significant improvements in R values. The two distances determined (2.34 and 2.41 Å for **6** and 2.33 and 2.42 Å for **7**) are not quite separable within the resolution of the EXAFS technique, which is approximated by the relation[50] $\Delta R = \pi/2\Delta k$ for scatterers of the same atomic number and which for the fitting range 3.5−19.5 $Å^{-1}$ would correspond to a ΔR of 0.10 Å. At this long distance, the Mo−N waves are, however, not dominant contributors to the total EXAFS signal and thus are not easily determined. For complexes **8** and **9**, the same coordination spheres at distances essentially identical to those seen in **6** and **7** were established. Individual EXAFS contributions and the total EXAFS signals and fits for **7** and **9** are shown in Figure 10. The excellent fits to the data evident here apply

(38) Lapasset, J.; Chezeau, N.; Belougne, P. *Acta Crystallogr.* **1976**, *B32*, 3087.
(39) To test the effect of ring formation on Mo−N distances, the sulfido derivative of **5** was sought. The reaction product proved to be somewhat unstable, and suitable crystals were not obtained.
(40) Eagle, A. A.; Harben, S. M.; Tiekink, E. R. T.; Young, C. G. *J. Am. Chem. Soc.* **1994**, *116*, 9749.
(41) Potvin, C.; Manoli, J. M.; Marzak, S.; Secheresse, F. *Acta Crystallogr.* **1988**, *C44*, 369.
(42) Coucouvanis, D.; Al-Ahmad, S.; Kim, C. G.; Mosier, P. E.; Kampf, J. W. *Inorg. Chem.* **1993**, *32*, 1533.
(43) Kawaguchi, H.; Yamada, K.; Lang, J.-P.; Tatsumi, K. *J. Am. Chem. Soc.* **1997**, *119*, 10346.
(44) Cotton, F. A.; Schmid, G. *Inorg. Chem.* **1997**, *36*, 2267.
(45) Xin, X.; Morris, N. L.; Jameson, G. B.; Pope, M. T. *Inorg. Chem.* **1985**, *24*, 3482.
(46) Coucouvanis, D.; Koo, S.-M. *Inorg. Chem.* **1989**, *28*, 2.
(47) Do, Y.; Simhon, E. D.; Holm, R. H. *Inorg. Chem.* **1985**, *24*, 2827.
(48) Serezhkin, V. N. *Russ. J. Inorg. Chem.* (*Engl. Transl.*) **1977**, *22*, 845.
(49) Gonschorek, W.; Hahn, T.; Müller, A. *Z. Kristallogr.* **1973**, *138*, 380.
(50) Shulman, R. G.; Eisenberger, P.; Blumberg, W. E.; Stombaugh, N. A. *Proc. Natl. Acad. Sci. U.S.A.* **1975**, *72*, 4003.

Table 3. GNXAS Fit Results of Mo K-Edge EXAFS[a]

	$[Mo^{VI}O_2(OSiPh_3)_2(phen)]$, **1**	$[Mo^{VI}OS(OSiPh_3)_2(phen)]$, **6**	$[Mo^{VI}OS(OSiPh_3)_2(Me_4phen)]$, **7**	$[Mo^{VI}OS(OSiPh_3)_2(4,4'\text{-}Me_2bipy)]$, **8**	$[Mo^{VI}OS(OSiPh_3)_2(5,5'\text{-}Me_2bipy)]$, **9**
E_0	20 018.4	20 017.7	20 017.9	20 017.6	20 017.0
S_0^2	0.953	0.954	0.953	0.951	0.950
R(Mo═O), Å	1.72	1.72	1.71	1.71	1.71
N[a]	2	1	1	1	1
σ^2, Å^2	0.001	0.001	0.001	0.002	0.001
R(Mo−O), Å	1.94	1.95	1.95	1.94	1.94
N[a]	2	2	2	2	2
σ^2, Å^2	0.003	0.005	0.004	0.002	0.003
R(Mo═S), Å		2.19	2.19	2.19	2.18
N[a]		1	1	1	1
σ^2, Å^2		0.002	0.002	0.002	0.001
R(Mo−N), Å	2.38	2.37	2.37	2.37	2.40
N[a]	2	2	2	2	2
σ^2, Å^2	0.003	0.004	0.004	0.005	0.003
R(O−Si), Å	1.62			1.65	1.68
N[a]	2			2	2
σ^2, Å^2	0.001			0.001	0.001
R(Mo−OSi), Å	3.52			3.53	3.54
MoOSi, deg	161 ± 2			159 ± 2	156 ± 3
R(N−C), Å	1.33			1.15	1.12
N[a]	2			2	2
σ^2, Å^2	0.002			0.001	0.001
R(Mo−NC), Å	3.23			3.28	3.28
MoNC, deg	120 ± 2			134 ± 4	134 ± 2
R (fit)	0.687×10^{-7}	0.273×10^{-7}	0.305×10^{-6}	0.315×10^{-7}	0.106×10^{-6}

[a] In the fits, the following parameters were refined: E_0, E_0^2, R(Mo═O, Mo−O, Mo═S, Mo−N, O−Si, N−C), and the corresponding σ^2 values as well as the six covariance matrix elements. The coordination numbers (N) were systematically varied throughout the analysis but were not allowed to vary in a given fit. The Γ_0 and experimental resolution parameters were fixed to physically reasonable values throughout the analysis. See the text for definitions of the above-mentioned parameters. The estimated standard deviations in bond distances are on the order of ±0.01−0.02 Å.

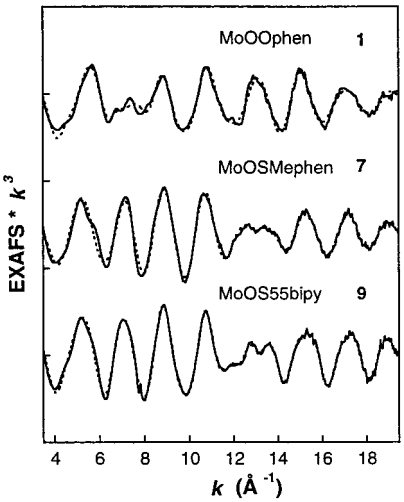

Figure 8. Comparison of the experimental EXAFS data (—) and fits to the data (- - -) for $[MoO_2(OSiPh_3)_2(phen)]$ (**1**, top), $[MoOS(OSiPh_3)_2(Me_4phen)]$ (**7**, middle), and $[MoOS(OSiPh_3)_2(5,5'\text{-}Me_2bpy)]$ (**9**, bottom). Significant differences in the EXAFS beat pattern around $k = 7$ and $k = 13$ Å^{-1} for **1** vs **7**/**9** are seen. (The ordinate scale is 10 units between each tick mark.)

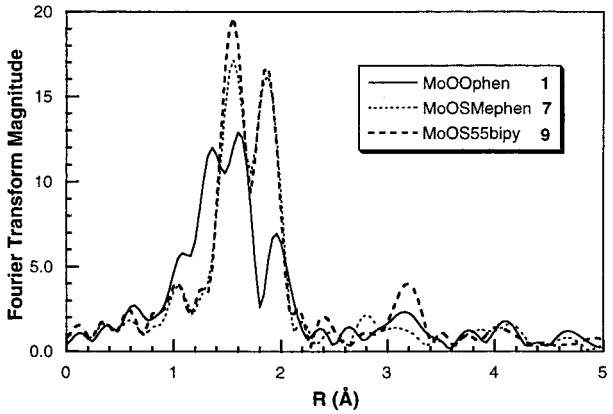

Figure 9. Comparison of the non-phase-shift-corrected Fourier transforms of $[MoO_2(OSiPh)_2(phen)]$ (**1**, —), $[MoOS(OSiPh_3)_2(Me_4phen)]$ (**7**, ···), and $[MoOS(OSiPh_3)_2(5,5'\text{-}Me_2bipy)]$ (**9**, - - -).

also to **1**, **6**, and **8**. The estimated standard deviations in the bond distances in Table 3 are ±(0.01−0.02) Å.

The Fourier transforms of the data for **1** and **8**/**9** (Figure 9) showed a distinctive peak at $R \sim 3.2$ Å. It is readily shown that, by inclusion of an Mo−O−Si multiple-scattering pathway modeled from the crystal structure (for **1**) and a similar arrangement (for **8**/**9**), this feature is well fit, with accompanying significant decreases in the fit function R from 0.112×10^{-6} to 0.790×10^{-7}, 0.940×10^{-7} to 0.467×10^{-7}, and 0.274×10^{-6} to 0.167×10^{-6} for **1**, **8**, and **9**, respectively, with resulting angles of ∼160°. While a strong improvement was seen, a small beat pattern remained in the EXAFS fit residual for all three complexes that was assumed to originate from Mo−N−C scattering from either the phenanthroline (**1**) or the bipyridyl (**8**, **9**) ring structure. Upon inclusion of this additional Mo−N−C multiple scattering pathway, a less significant decrease in the R value resulted. As an angle deviates further from linearity, the multiple-scattering signal contributes less to the total EXAFS wave and limits the possibility of detection. In all cases, the angles determined were low (120 and 134° for **1** and **8**/**9**, respectively) as was the multiplicity (2). All distances and their corresponding bond variances, as well as the nonstructural parameters that were allowed to float during the fitting, remained essentially constant in both the single- and multiple-scattering fits, implying that in either case the parameters were well fit.

It is interesting that an Mo−O−Si multiple-scattering interaction is not detected for complexes **6** and **7**, as may be deduced from the Fourier transform of **7** (Figure 9). In order that multiple

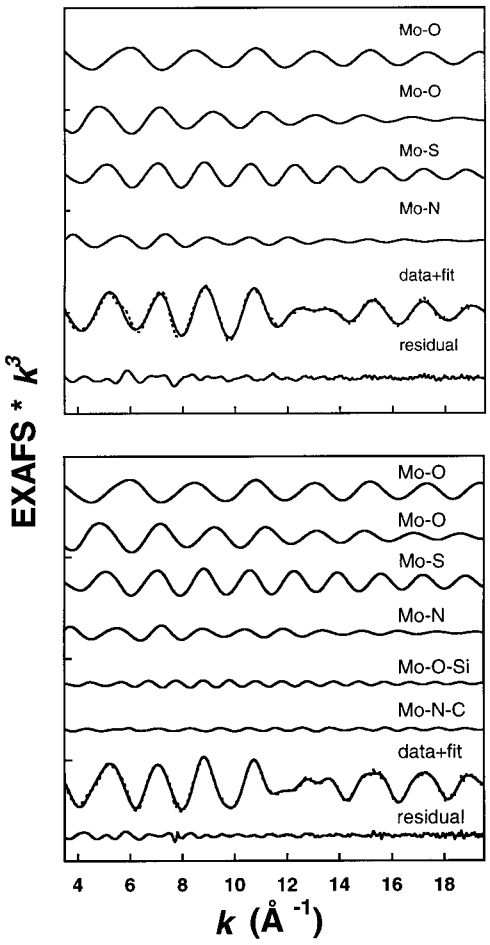

Figure 10. Individual EXAFS contributions and the total EXAFS signal (—) compared with the experimental EXAFS data (- - -) for $[MoOS(OSiPh_3)_2(Me_4phen)]$ (**7**, top) and $[MoOS(OSiPh_3)_2(5,5'\text{-}Me_2bipy)]$ (**9**, bottom). In both cases, the low residual is indicative of an excellent overall fit. (The ordinate scale is 15 units between each tick mark.)

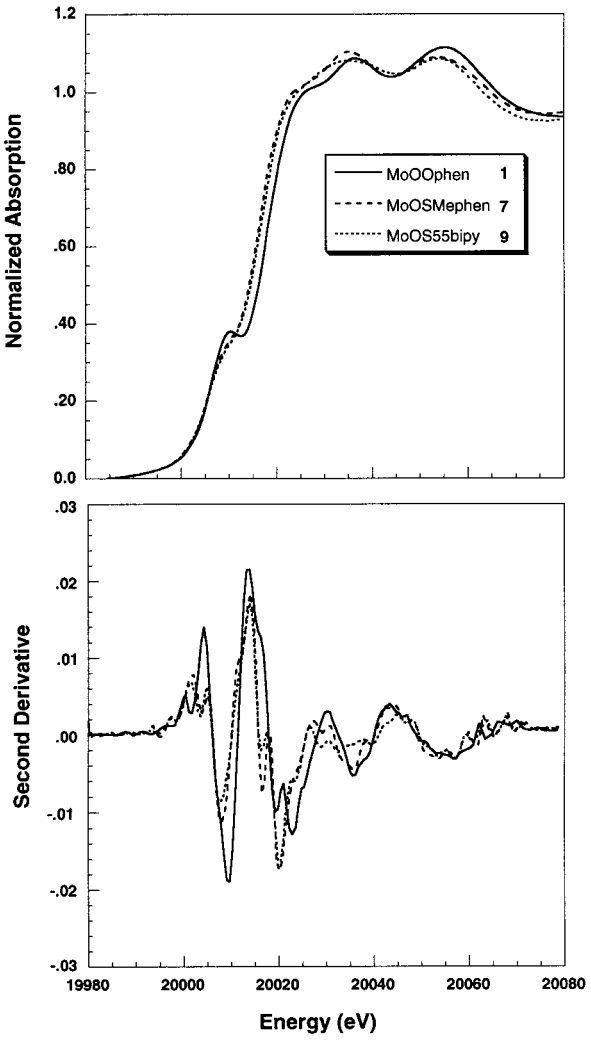

Figure 11. Normalized Mo K-edge spectra of $[MoO_2(OSiPh_3)_2(phen)]$ (**1**, —), $[MoOS(OSiPh_3)_2(Me_4phen)]$ (**7**, - - -), and $[MoOS(OSiPh_3)_2(5,5'\text{-}Me_2bipy)]$ (**9**, ···) with the corresponding second-derivative spectra shown below. See the text for a detailed description of the edge structure.

scattering contribute strongly to the EXAFS wave, it must involve rigidly fixed atoms in an almost linear arrangement. The bond variance parameters for the Mo−O distance in **6** and **7** are relatively high (0.004−0.005 Å^2) and are larger than those for the other three complexes (0.002−0.003 Å^2) in which the Mo−O−Si interaction was found to be significant. This may indicate that there is more static disorder present which decreases the multiple-scattering contribution. It is also possible that the reduced intensity signal is destructively interfering with the Mo−N−C multiple-scattering pathways, as opposed to the more constructive interference patterns seen in complexes **1**, **8**, and **9**. This effect produces cancellation of the contribution and prevents its detection. In any case, entirely satisfactory fits were obtained for both **7** and **9** (Figures 8 and 10).

A series of fits were performed for complexes **6**−**9** in which either the Mo═O or Mo═S interaction was not included, as well as fits in which the Mo═O, Mo−O, and Mo═S coordination numbers were varied. When the coordination number of either the Mo═O or the Mo═S interaction was increased above 1 or that of the Mo−O interaction was increased above 2, a large increase (to 0.008−0.011 Å^2) was seen in the bond variance parameter, essentially eliminating the coordination number increase. In fits for **7**, there was a decrease of approximately an order of magnitude in the *R* value, from a high of 0.301×10^{-5}, when two Mo═O interactions were included, to a low of 0.376×10^{-6}, for the best fit, in which oxo/sulfido ligation was included. In all cases, visually unacceptable fits to the data resulted without inclusion of both the Mo═O and Mo═S interactions. The conclusion is inescapable that *both Mo═O and Mo═S interactions are absolutely necessary to achieve acceptable EXAFS fits for complexes* ***6***−***9***.

(b) Molybdenum K Edges. Edge data for **1**, **7**, and **9** are shown in Figure 11 together with their second derivatives. The edges of complexes **6** and **7** are almost entirely superimposable as are those of **8** and **9**. These two sets of complexes are also strongly similar in the shapes and intensities of the edge transitions. The rising edges of **7** and **9** are shifted to lower energy by ∼2 eV relative to that of **1**. Such a shift is consistent with the higher electronegativity of oxygen, which results in differentially larger removal of electron density from the Mo(VI) center in **1**. The edge structure of this complex consists of at least four clearly displayed transitions (as confirmed by the second derivative) which are superimposed on the rising edge at ∼20 008, 20 017, 20 020, and 20 036 eV. As expected, the intensities and shapes of these edge transitions are very similar for **7** and **9**. The first three transitions of complex **1** are shifted to higher energy by ∼2 eV but have intensities relatively similar to those of complexes **7** and **9** with the exception of the transition at ∼20 010 eV, for which a substantial shift to higher energy as well a large increase in the intensity is seen.

Molybdenum complexes with Mo═O ligation show a characteristic edge feature around 20 008 eV. This arises from a formally dipole-forbidden 1s → 4d bound state transition to antibonding orbitals directed along the Mo═O bond(s) and gains intensity in noncentrosymmetric geometries through p mixing.[17,51] The Mo═S unit also contributes to this edge feature, but to a lesser extent with broader and less resolvable transitions.[17] The intensity and position of this transition can be correlated to the presence of one or two Mo═O groups.[52,53] The present set of complexes exhibit this "oxo" transition, which is most easily seen in the second-derivative spectra (Figure 11). The differences described above are thus in agreement with **1** containing two Mo═O bonds and **7** and **9** containing one Mo═O and one Mo═S bond, consistent with the EXAFS results.

Taken together, the EXAFS and edge analyses as well as the Fourier transforms are consistent with the existence of the oxo−sulfido functional group *cis*-Mo^{VI}OS, which is found in the xanthine oxidase family of molybdoenzymes. The Mo═O and Mo═S bond lengths determined in the X-ray refinement of disordered structures differ by 0.11 and 0.07 Å for **6** and by 0.06 and 0.01 Å for **7** from the respective EXAFS distances. While the X-ray distances cannot be said to be implausible, particularly those of **7**, they do not exhibit the conformity expected for such closely related molecules. Note that, for the set **6**−**9**, the individual Mo═O (1.71−1.72 Å) and the Mo═S values (2.18−2.19 Å) from EXAFS are not distinguishable. X-ray structures for **8** and **9** are unavailable. We conclude that the more reliable Mo═O and Mo═S bond lengths are those from the EXAFS analysis. X-ray diffraction defines the overall stereochemistry and other distance and angular features of the molecules. Bond lengths from both X-ray and EXAFS analyses are presented here as an illustration of a problem associated with O/S disorder and an experimental recourse necessary to obtain accurate values. The preferred distances compare favorably with those for the EXAFS consensus structure of xanthine oxidase (Mo═O 1.68 Å, Mo═S 2.15 Å)[1,4−6] and with those calculated from density functional theory for the five-coordinate unit [Mo^{VI}OS($S_2C_2H_2$)(OH_2)] (Mo═O 1.73 Å, Mo═S 2.18 Å).[54]

Oxo Abstraction of the Mo^{VI}OS Group. This group presents two atoms that are susceptible to nucleophilic attack with attendant reduction to Mo(IV). To ascertain which atom is removed by a nucleophile that is both oxophilic and thiophilic, equimolar amounts of **7** and Ph_3P were allowed to react in CD_2Cl_2 solution. After ca. 1 h, the ^{31}P NMR spectrum showed a strong signal for Ph_3PS (δ 46.7) and no signals for Ph_3PO (δ 35.3) or unreacted phosphine (δ −2.0).[55] When the experiment was conducted on a preparative scale, 37 μmol of **7** and 1.0 equiv of Ph_3P were allowed to react in 2 mL of dichloromethane. Within minutes, the orange solution became red; addition of ether resulted in precipitation of the reaction product, which after drying was obtained as a red solid. The product was identified as the Mo(V) complex **10** from the structure determination shown in Figure 12. As indicated in Figure 2, this complex is presumably formed by atom transfer to produce

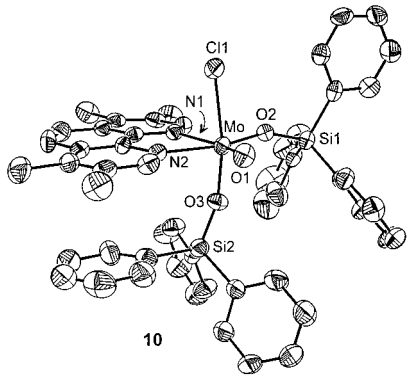

Figure 12. Structure of [MoOCl($OSiPh_3$)$_2$(Me_4phen)] (**10**) showing 50% probability ellipsoids and the atom-labeling scheme.

[Mo^{IV}O($OSiPh_3$)$_2$(Me_4phen)], which is then trapped by a chlorine atom transfer reaction with solvent to afford **10** in 63% yield.

Complex **10** has a distorted octahedral configuration in which the two silyloxy groups are cis to each other and cis to the oxo ligand, which itself is cis to chlorine. Consequently, the molecule does not have pseudo-2-fold symmetry and is not disordered. The Mo═O (1.703(4) Å) and Mo−Cl (2.434(2) Å) bond lengths and the Cl−Mo−O bond angle (95.4(1)°) are normal, as are the remaining metric parameters listed in Table 2. A small trans influence of the oxo ligand (0.08 Å) is evident in the Mo−N1 bond. In dichloromethane solution at 4.2 K, **10** exhibits a rhombically broadened EPR signal with $g \approx 1.95, 1.93, 1.89$.

The oxo abstraction reaction of **10** is controlled by the relative energies of the Mo^{VI}═O and Mo^{VI}═S bonds rather than the difference in P−element bond dissociation energies. The BDE of gaseous Ph_3PO is 133 kcal/mol[56] and that of Ph_3PS in benzene/toluene solution is 88 kcal/mol,[57] a difference of 45 kcal/mol. Recently, the BDE's of the four-coordinate Mo(V) complexes [MoQ(N[R]Ar)$_3$] were calorimetrically determined in solution.[58] The values are 156 kcal/mol for Q = O and 104 kcal/mol for Q = S. Other Mo═O BDE's have been determined or theoretically estimated to fall in the 126−158 kcal/mol range.[59−63] Density functional calculations afford BDE's of 126 and 79 kcal/mol for [$MoOCl_4$] and [$MoSCl_4$], respectively.[63] Although the data are limited and do not apply to six-coordinate Mo(VI), a reasonable conclusion at this stage is that Mo═O/Mo═S bond energy differences favor sulfur atom abstraction in the general case. Investigation of the reaction of **6** with Ph_3P and cyanide, a common deactivator of xanthine oxidase, in the absence of a trapping reagent is currently in progress.

Summary. The following are the principal results and conclusions of this investigation.

1. The complexes [MoOS($OSiPh_3$)$_2$(L-L)] with L-L a phenanthroline (**6**, **7**) or bipyridyl (**8**, **9**) ligand can be prepared by silylation of [MoO_3S]$^{2-}$ in the presence of L-L and isolated as orange solids in good yield.

(51) Kutzler, F. W.; Natoli, C. R.; Misemer, D. K.; Doniach, S.; Hodgson, K. O. *J. Chem. Phys.* **1980**, *73*, 3274.
(52) George, G. N.; Colangelo, C. M.; Dong, J.; Scott, R. A.; Khangulov, S. V.; Gladyshev, V. N.; Stadtman, T. C. *J. Am. Chem Soc.* **1998**, *120*, 1267.
(53) Musgrave, K. B.; Donahue, J. P.; Lorber, C.; Holm, R. H.; Hedman, B.; Hodgson, K. O. *J. Am. Chem. Soc*., submitted for publication.
(54) Voityuk, A. A.; Albert, K.; Köstlmeier, S.; Nasluzov, V. A.; Neyman, K. M.; Hof, P.; Huber, R.; Romão, M. J.; Rösch, N. *J. Am. Chem. Soc.* **1997**, *119*, 3159.
(55) ^{31}P chemical shifts are referenced to 85% D_3PO_4 in D_2O.
(56) Holm, R. H.; Donahue, J. P. *Polyhedron* **1993**, *12*, 571.
(57) Capps, K. B.; Wixmerten, B.; Bauer, A.; Hoff, C. D. *Inorg. Chem.* **1998**, *37*, 2861.
(58) Johnson, A. R.; Davis, W. M.; Cummins, C. C.; Serron, S.; Nolan, S. P.; Musaev, D. G.; Morokuma, K. *J. Am. Chem. Soc.* **1998**, *120*, 2071. N[R]Ar = $^{-}$NBu^t(3,5-$C_6H_3Me_2$).
(59) Glidewell, C. *Inorg. Chim. Acta* **1977**, *24*, 149.
(60) Pedley, J. B.; Marshall, E. M. *J. Phys. Chem. Ref. Data* **1983**, *12*, 967.
(61) Pershina, V.; Fricke, B. *J. Phys. Chem.* **1995**, *99*, 144; **1996**, *100*, 8748.
(62) The only exception is [$MoOCl_4$]; *D*(Mo═O) = 101 kcal/mol is calculated from thermodynamic data.[57]
(63) González-Blanco, O.; Branchadell, V.; Monteyne, K.; Ziegler, T. *Inorg. Chem.* **1998**, *37*, 1744.

2. The complexes in point 1 have been shown to contain the *cis*-$Mo^{VI}OS$ functional group from the collective evidence of elemental analyses, ^1H NMR spectra, mass spectrometry, X-ray structure determinations (**6**, **7**), Mo K-edge spectra, and EXAFS analyses. The orange color derives from a LMCT band at 424−434 nm.

3. Dioxo complexes $[MoO_2(OSiPh_3)_2(L\text{-}L)]$ approach or possess C_2 symmetry, with trans silyloxy groups cis to mutually cis oxo atoms. Oxo−sulfido complexes $[MoOS(OSiPh_3)_2(L\text{-}L)]$ have the same overall stereochemistry but exhibit O/S disorder in the crystalline state. X-ray structure refinements with O/S half-occupancies for complexes **6** and **7** afford Mo═O and Mo═S distances which, while not unreasonable, lack the internal consistency expected for such closely related molecules.

4. The distances in point 3 obtained for **6**−**9** by EXAFS analysis using the GNXAS protocol (Mo═O 1.71−1.72 Å, Mo═S 2.18−2.19 Å) are considered to be more reliable and are in good agreement with EXAFS values for xanthine oxidase. Both Mo═O and Mo═S interactions are absolutely necessary to obtain acceptable fits of the EXAFS data. Differences in Mo−N distances indicated by X-ray structures are not resolvable by EXAFS.

5. Reaction of $[MoOS(OSiPh_3)_2(Me_4phen)]$ with Ph_3P in dichloromethane affords $[Mo^{V}OCl(OSiPh_3)_2(Me_4phen)]$. Sulfur vs oxygen abstraction is favored by relative Mo═O/Mo═S bond energies and is likely to be a general result.

6. The results presented here demonstrate access to the unperturbed *cis*-$Mo^{VI}OS$ functional group obligatory for the activity of the xanthine oxidase family of enzymes. Complexes **6**−**9** or related species should allow further exploration of the structural and reactivity properties of this group. The method of synthesis may allow introduction of other, more biologically relevant ligands.

Acknowledgment. This research was supported by Grants NSF CHE 94-23181 and NIH RR-01209 (to K.O.H.) and NSF CHE 94-23830 (to R.H.H.) and by grants from the Swedish Natural Science Research Council and the Swedish Department of Education (to E.N.). The Stanford Synchrotron Radiation Laboratory is supported by the Department of Energy, Office of Basic Energy Sciences. The Biotechnology Program is supported by the National Institutes of Health, National Center for Research Resources, Biomedical Technology Program, and by the DOE Office of Biological and Environmental Research.

Supporting Information Available: Listings of crystallographic data for the compounds in Tables 1 and 2, including intensity collection details, positional and thermal parameters, interatomic distances and angles, and calculated hydrogen atom positions. This material is available free of charge via the Internet at http://pubs.acs.org.

IC990440V